Journal of Computational Physics **181,** 478–498 (2002)
doi:10.1006/jcph.2002.7138

Highly Energy-Conservative Finite Difference Method for the Cylindrical Coordinate System

Koji Fukagata*,† and Nobuhide Kasagi*

*Department of Mechanical Engineering, The University of Tokyo, 7-3-1 Hongo, Bunkyo-ku, Tokyo 113-8656, Japan; and †Institute for Energy Utilization, AIST, 1-2-1 Namiki, Tsukuba-shi, Ibaraki 305-8564, Japan
E-mail: fukagata@thtlab.t.u-tokyo.ac.jp

Received November 5, 2001; revised June 3, 2002

A highly energy-conservative second-order-accurate finite difference method for the cylindrical coordinate system is developed. It is rigorously proved that energy conservation in discretized space is satisfied when appropriate interpolation schemes are used. This argument holds not only for an unequally spaced mesh but also for an equally spaced mesh on cylindrical coordinates but not on Cartesian coordinates. Numerical tests are undertaken for an inviscid flow with various schemes, and it turns out that the proposed scheme offers a superior energy-conservation property and greater stability than the intuitive and previously proposed methods, for both equally spaced and unequally spaced meshes.

Key Words: finite difference method; cylindrical coordinate system; pipe flow; incompressible flow; energy conservation; advection; body force; singularity.

1. INTRODUCTION

With continuous development of high-performance computers, direct numerical simulation (DNS) and large eddy simulation (LES) have become very popular and even inevitable tools for turbulence research [1–4]. In general, the finite difference (FDM) and finite element (FEM) methods are used in these computations, while for special configurations with directional homogeneity, such as homogeneous turbulence and channel flow, very accurate simulation can be performed using the spectral method [5].

One of the most important requirements in FDM-based DNS/LES of incompressible flows is the flux and energy-conservation property of the discretized advection terms. Without a sufficient degree of flux and energy conservation in discretized space, computations may become unstable and eventually diverge. The idea of energy conservation in discretized space was addressed in the earliest stage of the development of numerical schemes and was then applied to the establishment of an energy-conservative second-order-accurate FDM on an equally spaced mesh in Cartesian coordinates [6, 7]. However, for a long time, it was

0021-9991/02 $35.00

unclear whether such energy-conservative schemes exist for higher order finite difference schemes, for unequally spaced mesh, or for coordinate systems other than Cartesian.

Recently, Morinishi *et al.* [8] generalized higher order finite difference schemes as relevant combinations of second-order finite differences defined on different stencils and succeeded in developing energy-conservative fourth-order-accurate finite difference schemes on various (regular, staggered, collocate) meshes. On the other hand, Kajishima [9] carefully examined the use of unequally spaced Cartesian staggered meshes and proposed energy-conservative second-order finite difference schemes for both the gradient and divergence forms of nonlinear terms in Navier–Stokes equations; they are proved to be valid even for unequally spaced mesh. According to Kajishima's [9] analysis, energy-conservative schemes on an unequally spaced mesh can be constructed only when relevant interpolation schemes are applied. A similar conclusion concerning spatial discretization is obtained in the very recent work by Ham *et al.* [10], who developed an energy-conservation scheme also in time discretization.

FDM-based DNS/LES in the cylindrical coordinate system has been reported by several workers. Various schemes have been proposed to remove singularity at the cylindrical axis ($r = 0$). Eggels *et al.* [11] and Akselvoll and Moin [12] used a second-order-accurate FDM with a staggered mesh system. They used the primitive variables, i.e., u_r, u_θ, u_z, and p, and resolved the singularity by defining the value of u_r at the axis as an average of those at the two grid points sandwiching the axis. Verzicco and Orlandi [13] proposed using the flux variable in the radial direction, $q_r = (ru_r)$, to avoid calculating u_r at the axis, and demonstrated the validity of their techniques in DNS of turbulent flow in a rotating pipe [14]. Very recently, Constantinescu and Lele [15], based on general series expansion around a singular point, proposed a very accurate treatment at the axis, which is suitable to higher order FDMs.

In the recent studies of FDMs in cylindrical coordinates [13, 15, 16], focus has been put mainly on the treatment of singularity at the cylindrical axis. Energy conservation in discretized space such as that made for the Cartesian coordinates, however, has not been discussed in detail. Moreover, the advantages and disadvantages of the various schemes proposed, with respect to energy conservation, remain unclear. Therefore, the objectives of the present study are to examine such energy conservation for the widely used second-order-accurate FDM in the cylindrical coordinate system and to propose highly energy-conservative schemes for the advection and centrifugal/Coriolis terms and a resolution for the singularity at the axis.

The paper is organized in the following manner. The governing equation in cylindrical coordinates is introduced in Section 2. In Section 3, mathematical formulations of energy-conservative discretization and interpolation schemes are provided; a new treatment of the singularity at the axis is proposed in Section 4. The proposed schemes are numerically tested in Section 5. Finally, conclusions are derived in Section 6.

2. GOVERNING EQUATIONS

The governing equations for the motion of an incompressible fluid flow are the continuity and Navier–Stokes equations. In cylindrical coordinates, these equations read:

- Continuity equation:

$$\frac{1}{r}\frac{\partial (ru_r)}{\partial r} + \frac{1}{r}\frac{\partial u_\theta}{\partial \theta} + \frac{\partial u_z}{\partial z} = 0; \tag{1}$$

- Navier–Stokes equation:

$$\begin{aligned}
\frac{\partial u_r}{\partial t} &= h_r + b_r - \frac{\partial p}{\partial r} + \frac{1}{Re}\left[\frac{1}{r}\frac{\partial}{\partial r}r\frac{\partial u_r}{\partial r} - \frac{u_r}{r^2} + \frac{1}{r^2}\frac{\partial^2 u_r}{\partial \theta^2} + \frac{\partial^2 u_r}{\partial z^2} - \frac{2}{r^2}\frac{\partial u_\theta}{\partial \theta}\right], \\
\frac{\partial u_\theta}{\partial t} &= h_\theta + b_\theta - \frac{1}{r}\frac{\partial p}{\partial \theta} + \frac{1}{Re}\left[\frac{1}{r}\frac{\partial}{\partial r}r\frac{\partial u_\theta}{\partial r} - \frac{u_\theta}{r^2} + \frac{1}{r^2}\frac{\partial^2 u_\theta}{\partial \theta^2} + \frac{\partial^2 u_\theta}{\partial z^2} + \frac{2}{r^2}\frac{\partial u_r}{\partial \theta}\right], \\
\frac{\partial u_z}{\partial t} &= h_z - \frac{dP}{dz} - \frac{\partial p}{\partial z} + \frac{1}{Re}\left[\frac{1}{r}\frac{\partial}{\partial r}r\frac{\partial u_z}{\partial r} + \frac{1}{r^2}\frac{\partial^2 u_z}{\partial \theta^2} + \frac{\partial^2 u_z}{\partial z^2}\right].
\end{aligned} \tag{2}$$

Here, the equations are nondimensionalized by using the pipe diameter R, the characteristic velocity U, and the kinematic viscosity of fluid ν. The Reynolds number is defined by

$$Re = \frac{UR}{\nu}. \tag{3}$$

The characteristic velocity, U, should be defined as either the friction velocity, $u_\tau = \sqrt{\tau_w/\rho}$, or the laminar centerline velocity, U_{lc}, depending on the flow condition, i.e., whether the mean pressure gradient, $-dP/dz$, or the mass flow rate is kept constant over the time of integration.

The first terms, h_r, h_θ, and h_z, on the right-hand side of the Navier–Stokes equation denote the advection terms, i.e.,

$$\begin{aligned}
h_r &= -\frac{1}{r}\frac{\partial}{\partial r}(ru_ru_r) - \frac{1}{r}\frac{\partial}{\partial \theta}(u_\theta u_r) - \frac{\partial}{\partial z}(u_z u_r), \\
h_\theta &= -\frac{1}{r}\frac{\partial}{\partial r}(ru_ru_\theta) - \frac{1}{r}\frac{\partial}{\partial \theta}(u_\theta u_\theta) - \frac{\partial}{\partial z}(u_z u_\theta), \\
h_z &= -\frac{1}{r}\frac{\partial}{\partial r}(ru_ru_z) - \frac{1}{r}\frac{\partial}{\partial \theta}(u_\theta u_z) - \frac{\partial}{\partial z}(u_z u_z).
\end{aligned} \tag{4}$$

The second terms, b_r and b_θ, in the equations of the r and θ directions are the centrifugal and Coriolis forces arising due to the curvature of the coordinate system, respectively, i.e.,

$$\begin{aligned}
b_r &= \frac{u_\theta^2}{r}, \\
b_\theta &= -\frac{u_r u_\theta}{r}.
\end{aligned} \tag{5}$$

3. RELEVANT SPATIAL DISCRETIZATION AND INTERPOLATION

3.1. Computational Mesh

In the present study, we focus only on the most frequently used method—the second-order-accurate finite difference scheme with a staggered mesh system. As usual, velocities are defined on the cell surfaces and pressure is defined at the cell centers as shown in Fig. 1. As a practically useful choice, the spacing is assumed to be equal in the θ and z

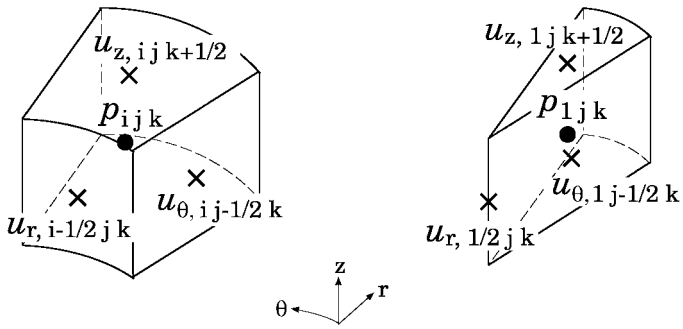

FIG. 1. Definition point of each variable. Ordinary cell (left) and the first cell from the center (right).

directions and unequal in the r direction. The definition of notations for the positions and mesh spacings in the r direction is shown in Fig. 2.

3.2. Advection Term

The advection terms given by Eq. (4) can be discretized so that the flux conservation is satisfied. For instance, the advection term in the r-direction, h_r, can be discretized as

$$\begin{aligned} h_{r,i+\frac{1}{2}jk} = &-\frac{1}{r_{i+\frac{1}{2}}}\frac{(ru_r)_{i+1jk}u_{r,i+1jk} - (ru_r)_{ijk}\,u_{r,ijk}}{\Delta r_{i+\frac{1}{2}}} \\ &-\frac{1}{r_{i+\frac{1}{2}}}\frac{u_{\theta,i+\frac{1}{2}j+\frac{1}{2}k}\,u_{r,i+\frac{1}{2}j+\frac{1}{2}k} - u_{\theta,i+\frac{1}{2}j-\frac{1}{2}k}\,u_{r,i+\frac{1}{2}j-\frac{1}{2}k}}{\Delta\theta} \\ &-\frac{u_{z,i+\frac{1}{2}jk+\frac{1}{2}}\,u_{r,i+\frac{1}{2}jk+\frac{1}{2}} - u_{z,i+\frac{1}{2}jk-\frac{1}{2}}\,u_{r,i+\frac{1}{2}jk-\frac{1}{2}}}{\Delta z}, \end{aligned} \tag{6}$$

where $\Delta r_{i+\frac{1}{2}}$ is defined in Fig. 2. The above equation contains undefined velocities such as $u_{r,ijk}$ and $u_{\theta,i+\frac{1}{2}j+\frac{1}{2}k}$. Therefore, we need to evaluate them by interpolation of the defined velocities. A common practice is to use an arithmetic average or a linear interpolation. With

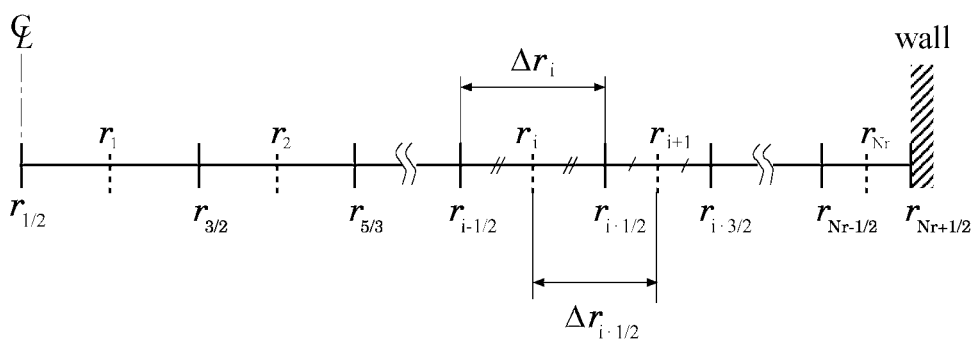

FIG. 2. Definition of the positions, r_i and $r_{i+\frac{1}{2}}$, and the local mesh spacings, Δr_i and $\Delta r_{i+\frac{1}{2}}$.

an arithmetic average, for example, Eq. (6) simply becomes

$$
\begin{aligned}
h_{r,i+\frac{1}{2}jk} = &-\frac{1}{r_{i+\frac{1}{2}}}\frac{\overline{(ru_r)}^{i}_{i+1jk}\overline{u_r}^{i}_{i+1jk} - \overline{(ru_r)}^{i}_{ijk}\overline{u_r}^{i}_{ijk}}{\Delta r_{i+\frac{1}{2}}} \\
&-\frac{1}{r_{i+\frac{1}{2}}}\frac{\overline{u_\theta}^{i}_{i+\frac{1}{2}j+\frac{1}{2}k}\overline{u_r}^{j}_{i+\frac{1}{2}j+\frac{1}{2}k} - \overline{u_\theta}^{i}_{i+\frac{1}{2}j-\frac{1}{2}k}\overline{u_r}^{j}_{i+\frac{1}{2}j-\frac{1}{2}k}}{\Delta\theta} \\
&-\frac{\overline{u_z}^{i}_{i+\frac{1}{2}jk+\frac{1}{2}}\overline{u_r}^{k}_{i+\frac{1}{2}jk+\frac{1}{2}} - \overline{u_z}^{i}_{i+\frac{1}{2}jk-\frac{1}{2}}\overline{u_r}^{k}_{i+\frac{1}{2}jk-\frac{1}{2}}}{\Delta z},
\end{aligned}
\tag{7}
$$

where the overbar, $\overline{\cdot}^{\ell}$, denotes the arithmetic average, and the superscript to the overbar, ℓ, represents the direction of interpolation, e.g.,

$$
\begin{aligned}
\overline{(ru_r)}^{i}_{ijk} &= \frac{(ru_r)_{i+\frac{1}{2}jk} + (ru_r)_{i-\frac{1}{2}jk}}{2}, \\
\overline{u_r}^{j}_{i+\frac{1}{2}j+\frac{1}{2}k} &= \frac{u_{r,i+\frac{1}{2}j+1k} + u_{r,i+\frac{1}{2}jk}}{2}.
\end{aligned}
\tag{8}
$$

However, according to the recent analyses on FDMs in Cartesian coordinates [9, 10, 17], energy conservation is violated in discretized space when an unequally spaced mesh is employed and the arithmetic average or the linear interpolation is used on it. This is due to an inconsistency between the differencing and interpolating operators [17]. In order to overcome this problem, Kajishima [9] treated the unequally spaced rectangular mesh x_m $(m = 1, 2, 3)$ as a mapping from an equally spaced mesh ξ^m. The divergence form of the advection term was approximated by

$$
\frac{\partial u_m u_n}{\partial x_n} = \frac{1}{J}\frac{\partial (JU^n u_m)}{\partial \xi^n} = \frac{1}{J}\frac{\delta\left(\overline{JU^n}^{m}\overline{u_m}^{n}\right)}{\delta\xi^n},
\tag{9}
$$

where $U^n = u_\ell \partial\xi^n/\partial x_\ell$ is the contravariant velocity and $\delta/\delta\xi^n$ is the second-order central difference on the ξ^n mesh. The Jacobian in the mapping is denoted as J. Energy conservation by this approximation was then verified on a two-dimensional Cartesian mesh by a procedure similar to that shown below. It is also worth noting that such a relevant interpolation rule makes the divergence form and the gradient form of the advection term compatible in discretized space. This was also verified by the fact that two different numerical simulations of a two-dimensional cavity flow (one of them adopted the divergence form for the nonlinear term; the other, the gradient form) gave the same results. On the other hand, Ham *et al.* [10] approximated the nonlinear term as

$$
\frac{\partial u_m u_n}{\partial x_n} = \frac{\delta\widehat{u_n}^{m}\overline{u_m}^{n}}{\delta x_n},
\tag{10}
$$

where $\widehat{\cdot}^{\ell}$ is an average weighted by the overlapping volume of the cell where the velocity is defined and of the cell where it is interpolated (referred to hereafter as the volume-flux average), and verified the energy-conservation property on an unequally spaced rectangular mesh. It can be easily noticed that these two expressions, Eqs. (9) and (10), are identical when they are expressed in concrete form in Cartesian coordinates. Therefore, the relevant

interpolation schemes for the energy to be conserved can be summarized as:

- volume-flux average—for the *advecting* velocity;
- arithmetic average—for the *advected* velocity.

Here, the terms *advecting* and *advected* are used for notational convenience. Their meanings are the same as those used for the gradient forms of nonlinear terms in the Navier–Stokes equation: in Eq. (6), for example, (ru_r), u_θ, and u_z are the *advecting* velocities and u_r is the *advected* velocity.

We apply this interpolation rule to the discretized equation in the cylindrical coordinates. As one can see in the verification process below, the key technique (or trick) in the present case is to arrange the right-hand side in such a form that every term has a common denominator, i.e., $r_{i+\frac{1}{2}}\Delta r_{i+\frac{1}{2}}$. As a result, Eq. (4) reads

$$\begin{aligned} h_{r,\,i+\frac{1}{2}jk} = &-\frac{1}{r_{i+\frac{1}{2}}\Delta_{ri+\frac{1}{2}}}\left[\overline{(ru_r)}^{\,i}_{i+1jk}\,\overline{u_r}^{\,i}_{i+1jk} - \overline{(ru_r)}^{\,i}_{ijk}\,\overline{u_r}^{\,i}_{ijk}\right] \\ &-\frac{1}{r_{i+\frac{1}{2}}\Delta\theta}\left[\widehat{u_\theta}^{\,i}_{i+\frac{1}{2}j+\frac{1}{2}k}\,\overline{u_r}^{\,j}_{i+\frac{1}{2}j+\frac{1}{2}k} - \widehat{u_\theta}^{\,i}_{i+\frac{1}{2}j-\frac{1}{2}k}\,\overline{u_r}^{\,j}_{i+\frac{1}{2}j-\frac{1}{2}k}\right] \\ &-\frac{1}{\Delta z}\left[\widehat{u_z}^{\,i}_{i+\frac{1}{2}jk+\frac{1}{2}}\,\overline{u_r}^{\,k}_{i+\frac{1}{2}jk+\frac{1}{2}} - \widehat{u_z}^{\,i}_{i+\frac{1}{2}jk-\frac{1}{2}}\,\overline{u_r}^{\,k}_{i+\frac{1}{2}jk-\frac{1}{2}}\right], \end{aligned} \tag{11}$$

where $\widehat{\cdot}^{\,\ell}$ denotes the volume-flux average defined by

$$\widehat{u_\theta}^{\,i}_{i+\frac{1}{2}j+\frac{1}{2}k} = \frac{\Delta r_{i+1}u_{\theta,i+1j+\frac{1}{2}k} + \Delta r_i u_{\theta,ij+\frac{1}{2}k}}{2\Delta r_{i+\frac{1}{2}}} \tag{12}$$

and

$$\widehat{u_z}^{\,i}_{i+\frac{1}{2}jk+\frac{1}{2}} = \frac{r_{i+1}\Delta r_{i+1}u_{z,i+1jk+\frac{1}{2}} + r_i\Delta r_i u_{z,ijk+\frac{1}{2}}}{2r_{i+\frac{1}{2}}\Delta r_{i+\frac{1}{2}}\chi_{i+\frac{1}{2}}}. \tag{13}$$

In the present case, the volume-flux average for (ru_r) is, within second-order accuracy, identical to the arithmetic average. The normalization factor, $\chi_{i+\frac{1}{2}}$, in Eq. (13) is necessary so that the summation of the weighting factors becomes unity,

$$\chi_{i+\frac{1}{2}} = \frac{r_{i+1}\Delta r_{i+1} + r_i\Delta r_i}{2r_{i+\frac{1}{2}}\Delta r_{i+\frac{1}{2}}} = 1 + \frac{\Delta r_{i+1} - \Delta r_i}{2r_{i+\frac{1}{2}}}, \tag{14}$$

which, of course, is unity for an equally spaced mesh and close to unity for an unequally spaced mesh if the variations of Δr in the vicinity of the cylindrical axis are small. Note that the weighting factors due to mesh spacings, Δr_i and Δr_{i+1}, in Eqs. (12) and (13) are the opposite of those in the linear interpolation. Moreover, it is emphasized that the present expression, Eq. (11), and that with the arithmetic average, Eq. (7), are not identical even when the mesh spacing is equal, i.e., $\Delta r_i = \Delta r_{i+1} = const.$; the flux weighting factors due to r_i and r_{i+1} still exist in the z-differential term. This situation is quite different from that in the Cartesian coordinate system [9, 10], where the arithmetic average and the relevant interpolation become identical in the case of an equally spaced mesh.

The terms in other directions, h_θ and h_z, can be discretized similarly. Under the present conditions, i.e., uniform mesh in the θ and z directions, the final expression of h_θ and h_z can

be obtained using the arithmetic average only. Hereafter, we refer to the form of Eq. (11) as (Div.-C), while the form obtained using the arithmetic average, Eq. (7), is referred to as (Div.-A).

The conservation of a squared value, u_r^2, i.e., a radial component of the kinetic energy, can be verified as follows. Similar to that in Eq. (11), the discretized advection term of the squared value can be written as:

$$\begin{aligned} H_{r,i+\frac{1}{2}jk} = &-\frac{1}{r_{i+\frac{1}{2}}\Delta r_{i+\frac{1}{2}}}\left[\overline{(ru_r)}^{i}_{i+1jk}\widetilde{\left(u_r^2\right)}^{i}_{i+1jk} - \overline{(ru_r)}^{i}_{ijk}\widetilde{\left(u_r^2\right)}^{i}_{ijk}\right] \\ &-\frac{1}{r_{i+\frac{1}{2}}\Delta\theta}\left[\widehat{u_\theta}^{i}_{i+\frac{1}{2}j+\frac{1}{2}k}\widetilde{\left(u_r^2\right)}^{j}_{i+\frac{1}{2}j+\frac{1}{2}k} - \widehat{u_\theta}^{i}_{i+\frac{1}{2}j-\frac{1}{2}k}\widetilde{\left(u_r^2\right)}^{j}_{i+\frac{1}{2}j-\frac{1}{2}k}\right] \\ &-\frac{1}{\Delta z}\left[\widehat{u_z}^{i}_{i+\frac{1}{2}jk+\frac{1}{2}}\widetilde{\left(u_r^2\right)}^{k}_{i+\frac{1}{2}jk+\frac{1}{2}} - \widehat{u_z}^{i}_{i+\frac{1}{2}jk-\frac{1}{2}}\widetilde{\left(u_r^2\right)}^{k}_{i+\frac{1}{2}jk-\frac{1}{2}}\right]. \end{aligned} \tag{15}$$

The squared values at undefined points are evaluated by following Piacsek and Williams [7], e.g.,

$$\begin{aligned} \widetilde{\left(u_r^2\right)}_{i,j,k} &= u_{r,i+\frac{1}{2}jk}u_{r,i-\frac{1}{2}jk}, \\ \widetilde{\left(u_r^2\right)}_{i+\frac{1}{2},j+\frac{1}{2},k} &= u_{r,i+\frac{1}{2}j+1k}u_{r,i+\frac{1}{2}jk}, \\ \widetilde{\left(u_r^2\right)}_{i+\frac{1}{2}jk+\frac{1}{2}} &= u_{r,i+\frac{1}{2}jk+1}u_{r,i+\frac{1}{2}jk}, \end{aligned} \tag{16}$$

and the normalization factor for the z-differential term, $\chi_{i+\frac{1}{2}}$, was approximated as unity. The transport equation of the squared value can also be obtained by multiplying $2u_{ri+\frac{1}{2},j,k}$ to Eq. (11). The former, i.e., Eq. (15), exactly represents the transport of the squared value, while the latter, i.e., $2(u_r h_r)_{i+\frac{1}{2}jk}$, expresses the squared value transport as a result of advection. Therefore, these two expressions must be identical in order for the discretized advection term to become energy-conservative. By subtracting Eq. (15) from $2(u_r h_r)_{i+\frac{1}{2}jk}$, one obtains

$$2(u_r h_r)_{i+\frac{1}{2}jk} - H_{r,i+\frac{1}{2}jk} = -\frac{r_{i+1}\Delta r_{i+1}u^2_{r,i+\frac{1}{2}jk}}{2r_{i+\frac{1}{2}}\Delta r_{i+\frac{1}{2}}}(\vec{\mathcal{D}}\cdot\vec{u})_{i+1jk} - \frac{r_i\Delta r_i u^2_{r,i+\frac{1}{2}jk}}{2r_{i+\frac{1}{2}}\Delta r_{i+\frac{1}{2}}}(\vec{\mathcal{D}}\cdot\vec{u})_{ijk}, \tag{17}$$

where $(\vec{\mathcal{D}}\cdot\vec{u})_{ijk}$ expresses the divergence of the discretized velocity field, i.e.,

$$(\vec{\mathcal{D}}\cdot\vec{u})_{ijk} = \frac{1}{r_i}\frac{(ru_r)_{i+\frac{1}{2}jk} - (ru_r)_{i-\frac{1}{2}jk}}{\Delta r_i} + \frac{1}{r_i}\frac{u_{\theta,ij+\frac{1}{2}k} - u_{\theta,ij-\frac{1}{2}k}}{\Delta\theta} + \frac{u_{z,ijk+\frac{1}{2}} - u_{z,ijk-\frac{1}{2}}}{\Delta z}. \tag{18}$$

Therefore, the squared value is perfectly conserved if the continuity is satisfied in the discretized space. The equations in the θ and z directions can also be verified in the same way.

It should be emphasized again that the scheme based on the arithmetic interpolation, i.e., (Div.-A) expressed by Eq. (7), is not energy-conserving even on the equally spaced mesh

($\Delta r_i = \Delta r$) in the cylindrical coordinates. An analysis similar to that in Eqs. (15)–(17) for the case of (Div.-A) results in

$$2(u_r h_r)_{i+\frac{1}{2}jk} - H_{r,i+\frac{1}{2}jk} = -\frac{r_{i+1}u^2_{r,i+\frac{1}{2}jk}}{2r_{i+\frac{1}{2}}}(\vec{\mathcal{D}}\cdot\vec{u})_{i+1jk} - \frac{r_i u^2_{r,i+\frac{1}{2}jk}}{2r_{i+\frac{1}{2}}}(\vec{\mathcal{D}}\cdot\vec{u})_{ijk} + \frac{\Delta r^2 u^2_{r,i+\frac{1}{2}jk}}{4r_{i+\frac{1}{2}}}\frac{\delta^2 u_z}{\delta r \delta z}\bigg|_{i+\frac{1}{2}jk}, \tag{19}$$

where $\delta/\delta r$ and $\delta/\delta z$ denote the usual second-order central difference. Equation (19) suggests that the energy-conservation property in (Div.-A) on the equally spaced mesh has a first-order inconsistency near the axis ($r \sim \Delta r$). Similar analyses for other schemes, e.g., (Div.-A) on an unequally spaced mesh or (Div.-F), which appears in the next section, also show that $2(u_r h_r)_{i+\frac{1}{2}jk}$ and $H_{r,i+\frac{1}{2}jk}$ are inconsistent, although the order of inconsistency cannot be expressed in a form as simple as Eq. (19). Therefore, only the combination of discretization and interpolation schemes described above, i.e., (Div.-C), seems to satisfy the conservation of squared values.

3.3. Body Force Term

The body force terms, b_r and b_θ, satisfy the following relation in continuous space:

$$u_r b_r + u_\theta b_\theta = 0. \tag{20}$$

This relation expresses the exchange of energy between r and θ components. Therefore, interpolation for these terms should be designed so as to satisfy this rigorous conservation rule in each 1/4 of a cell as shown in Fig. 3. The resulting form, referred to as

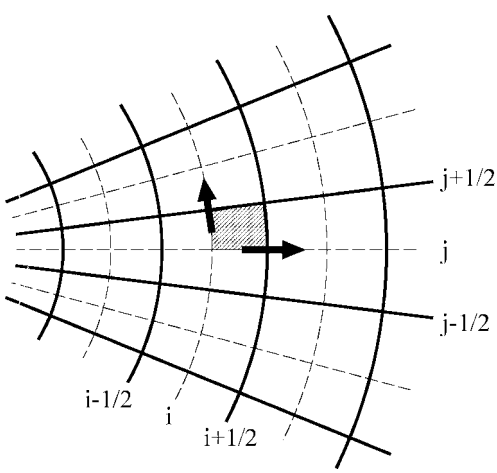

FIG. 3. Subregion of a control volume for u_r and u_θ (shaded). Energy exchange due to body force is conserved in each subregion.

(Body-C), is

$$b_{r,i+\frac{1}{2}jk} = \frac{1}{r_{i+\frac{1}{2}}} \frac{\Delta r_{i+1} \overline{\left(u_\theta^2\right)}^j_{i+1jk} + \Delta r_i \overline{\left(u_\theta^2\right)}^j_{ijk}}{2\Delta r_{i+\frac{1}{2}}},$$
$$b_{\theta,ij+\frac{1}{2}k} = -\frac{1}{r_i} \overline{\overline{u_r}^i}^j_{ij+\frac{1}{2}k} u_{\theta,ij+\frac{1}{2}k}. \tag{21}$$

Note, again, that the weighting factors are opposite to those in the linear interpolation.

It is unclear what kind of interpolation scheme was used in previous simulations. An intuitive method, however, is to approximate the undefined velocity simply by using an arithmetic average, which is referred to as (Body-A). In this case, the expression for b_θ is the same as Eq. (21), while that for b_r becomes

$$b_{r,i+\frac{1}{2}jk} = \frac{1}{r_{i+\frac{1}{2}}} \left(\overline{\overline{u_\theta}^i}^j_{i+\frac{1}{2}jk} \right)^2. \tag{22}$$

Clearly, the local energy conservation of Eq. (20) is not satisfied by (Body-A), even for the equally spaced mesh.

4. A NEW TREATMENT AT THE CYLINDRICAL AXIS

As mentioned in the introduction, an important resulting issue in simulations on cylindrical coordinates is the mathematical treatment of the singularity at $r = 0$. Most of the singularities appearing in the Navier–Stokes equation (Eq. (2)), are automatically removed after the spatial discretization using a second-order FDM with a staggered mesh system. Remaining ones are the radial velocity, $u_{r,\frac{1}{2}jk}$, to be used for

- interpolation in the advection term, h_r (Eq. (11)),
- interpolation in the body force term, b_θ (Eq. (21)),

and that used for discretization of the diffusion terms.

For this problem, two different approaches have been proposed to date:

1. An artificial velocity is defined as

$$u_{r,\frac{1}{2}jk} = \frac{1}{2}\left(u_{r,\frac{3}{2}jk} - u_{r,\frac{3}{2}j+\frac{N_\theta}{2}k} \right), \tag{23}$$

where N_θ is the number of meshes in the θ direction (referred to as (Axis-E)) [11].

2. The singularity is removed by multiplying the u_r momentum equation by r (the flux-based formulation) [13].

With the flux-based formulation, h_r and b_θ are discretized as

$$\begin{aligned}(rh_r)_{i+\frac{1}{2}jk} = &-\frac{1}{\Delta r_{i+\frac{1}{2}}} \left[\frac{1}{r_{i+1}} \overline{(ru_r)}^i_{i+1jk} \overline{(ru_r)}^i_{i+1jk} - \frac{1}{r_i} \overline{(ru_r)}^i_{ijk} \overline{(ru_r)}^i_{ijk} \right] \\ &- \frac{1}{r_{i+\frac{1}{2}}} \frac{\overline{u_\theta}^i_{i+\frac{1}{2}j+\frac{1}{2}k} \overline{(ru_r)}^j_{i+\frac{1}{2}j+\frac{1}{2}k} - \overline{u_\theta}^i_{i+\frac{1}{2}j-\frac{1}{2}k} \overline{(ru_r)}^j_{i+\frac{1}{2}j-\frac{1}{2}k}}{\Delta\theta} \\ &- \frac{\overline{u_z}^i_{i+\frac{1}{2}jk+\frac{1}{2}} \overline{(ru_r)}^k_{i+\frac{1}{2}jk+\frac{1}{2}} - \overline{u_z}^i_{i+\frac{1}{2}jk-\frac{1}{2}} \overline{(ru_r)}^k_{i+\frac{1}{2}jk-\frac{1}{2}}}{\Delta z},\end{aligned} \tag{24}$$

and

$$b_{\theta,ij+\frac{1}{2}k} = -\frac{1}{r_i^2}\overline{\overline{(ru_r)}^{i}}^{j}{}_{ij+\frac{1}{2}k} u_{\theta,i,j+\frac{1}{2}k}. \tag{25}$$

Since $(ru_r)_{\frac{1}{2}jk} = 0$, it does not require any approximation at the point of $r = 0$. However, based on this formulation, an energy-conservative scheme such as that in the previous section cannot be constructed. A modified method, in which the energy-conservative scheme is used, but with the flux-based formulation only at the first points from the axis, can also be considered. In that case, it can be found from Eq. (11) that it is equivalent to use the following artificial velocity (referred to as (Axis-F)):

$$u_{r,\frac{1}{2}jk} = u_{r,\frac{3}{2}jk}. \tag{26}$$

A schematic of the different treatments is shown in Fig. 4.

In the present study, a new method is proposed such that the mathematical constraint at $r = 0$,

$$\begin{aligned} u_r &= u_x \cos\theta + u_y \sin\theta, \\ u_\theta &= -u_x \sin\theta + u_y \cos\theta, \end{aligned} \tag{27}$$

should be satisfied. Here, u_x and u_y are velocity components expressed in Cartesian

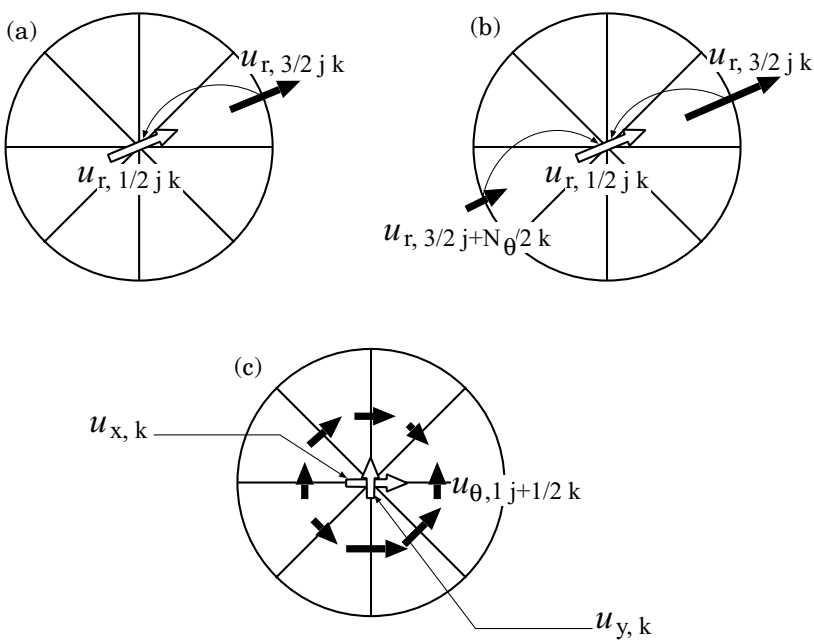

FIG. 4. Different treatments at a cylindrical axis. Vectors in black are those defined and actually solved; vectors in white are artificial ones at $r = 0$. (a) Method equivalent to flux-based formulation (Axis-F); (b) treatment by Eggels *et al*. [11] (Axis-E); (c) first step of the present method (Axis-C).

coordinates. As shown in Fig. 4c, the procedure to compute $u_{r,\frac{1}{2}jk}$ is given as follows:

1. Calculate u_x and u_y at $r=0$ from $u_{\theta,1j+\frac{1}{2}k}$.

$$\begin{aligned} u_{x,k} &= -\frac{2}{N_\theta}\sum_{j=0}^{N_\theta-1} u_{\theta,1j+\frac{1}{2}k}\sin\theta_j, \\ u_{y,k} &= \frac{2}{N_\theta}\sum_{j=0}^{N_\theta-1} u_{\theta,1j+\frac{1}{2}k}\cos\theta_j. \end{aligned} \tag{28}$$

2. Calculate $u_{r,\frac{1}{2}jk}$ by using Eq. (27):

$$u_{r,\frac{1}{2}jk} = u_{x,k}\cos\theta_j + u_{y,k}\sin\theta_j. \tag{29}$$

The accuracy order of the present procedure can easily be assessed. The series expansion of $u_{\theta,1j+\frac{1}{2}k}$, around the singular point, $r=0$, can be written [15, 18] as

$$\begin{aligned} u_{\theta,1j+\frac{1}{2}k} = {} & A_{01}^{(\theta)}\left(\frac{\Delta r_1}{2}\right) + \left[A_{10}^{(\theta)} + A_{11}^{(\theta)}\left(\frac{\Delta r_1}{2}\right)^2\right]\cos\theta_{j+\frac{1}{2}} + A_{20}^{(\theta)}\left(\frac{\Delta r_1}{2}\right)\cos 2\theta_{j+\frac{1}{2}} \\ & + B_{01}^{(\theta)}\left(\frac{\Delta r_1}{2}\right) + \left[B_{10}^{(\theta)} + B_{11}^{(\theta)}\left(\frac{\Delta r_1}{2}\right)^2\right]\sin\theta_{j+\frac{1}{2}} \\ & + B_{20}^{(\theta)}\left(\frac{\Delta r_1}{2}\right)\sin 2\theta_{j+\frac{1}{2}} + O\left(\Delta r_1^3\right), \end{aligned} \tag{30}$$

where $A_{mn}^{(\theta)}$ and $B_{mn}^{(\theta)}$ are coefficients for the corresponding modes. It is easily found that $A_{10}^{(\theta)}$ and $B_{10}^{(\theta)}$ are equivalent, respectively, to

$$\begin{aligned} A_{10}^{(\theta)} &= u_{y,k}, \\ B_{10}^{(\theta)} &= -u_{x,k}. \end{aligned} \tag{31}$$

Summation of Eq. (30) multiplied by $\cos\theta$ yields

$$\sum_{j=0}^{N_\theta-1} u_{\theta,1j+\frac{1}{2}k}\cos\theta_{j+\frac{1}{2}} = \frac{N_\theta}{2}\left[u_{y,k} + A_{11}^{(\theta)}\left(\frac{\Delta r_1}{2}\right)^2\right]. \tag{32}$$

Similarly,

$$\sum_{j=0}^{N_\theta-1} u_{\theta,1j+\frac{1}{2}k}\sin\theta_{j+\frac{1}{2}} = \frac{N_\theta}{2}\left[-u_{x,k} + B_{11}^{(\theta)}\left(\frac{\Delta r_1}{2}\right)^2\right]. \tag{33}$$

Therefore, the present interpolation procedure, Eq. (28), has second-order accuracy with respect to Δr_1.

Energy conservation around the cylindrical axis should also be investigated. By carrying out a derivation similar to that in the previous section, we find that an extra condition,

$$u_{r,\frac{3}{2}jk} + \frac{u_{\theta,1j+\frac{1}{2}k} - u_{\theta,1j-\frac{1}{2}k}}{\Delta\theta} = 0, \tag{34}$$

should be satisfied in order for the squared value to be conserved. From the series expansion similar to Eq. (30), one obtains

$$u_{r,\frac{3}{2}jk} + \frac{u_{\theta,1j+\frac{1}{2}k} - u_{\theta,1j-\frac{1}{2}k}}{\Delta\theta} = \left[A_{01}^{(r)} + B_{01}^{(r)} + \left(A_{20}^{(r)} - A_{20}^{(\theta)}\right)\cos 2\theta_j + \left(B_{20}^{(r)} - B_{20}^{(\theta)}\right)\sin 2\theta_j\right]\Delta r_1 + O\left(\Delta r_1^2, \Delta\theta^2\right), \tag{35}$$

which reveals that the present method has only first-order accuracy concerning the energy conservation around the cylindrical axis. However, we do not attempt to directly impose the condition of Eq. (34), because this or an equivalent condition under the continuity,

$$u_{z,1jk+\frac{1}{2}} - u_{z,1jk-\frac{1}{2}} = 0, \tag{36}$$

prohibits any variation of u_z along the longitudinal direction and is quite unphysical. The effects of this first-order error around the axis are shown to be minor in the next section because the size of volume influenced is considered small if compared to the rest of the domain.

5. NUMERICAL TEST

In order to demonstrate an energy-conservation property of the proposed schemes, numerical tests are conducted assuming an inviscid flow in a straight circular pipe, i.e., $Re \to \infty$, with no driving force, i.e., $-dP/dz = 0$. The reduced set of governing equations read:

- continuity equation:

$$\frac{1}{r}\frac{\partial(ru_r)}{\partial r} + \frac{1}{r}\frac{\partial u_\theta}{\partial\theta} + \frac{\partial u_z}{\partial z} = 0; \tag{37}$$

- momentum equation:

$$\begin{aligned} \frac{\partial u_r}{\partial t} &= h_r + b_r - \frac{\partial p}{\partial r}, \\ \frac{\partial u_\theta}{\partial t} &= h_\theta + b_\theta - \frac{1}{r}\frac{\partial p}{\partial\theta}, \\ \frac{\partial u_z}{\partial t} &= h_z - \frac{\partial p}{\partial z}. \end{aligned} \tag{38}$$

Tested different combinations of schemes for the advection term, body force term, and treatment at the axis are summarized in the following:

- advection term:
  (Div.-C) present scheme (Eq. (11)),
  (Div.-A) arithmetic average (Eq. (7)),
  (Div.-F) flux-based formulation (Eq. (24));
- body force term:
  (Body-C) present scheme (Eq. (21)),
  (Body-A) arithmetic average (Eq. (22)),
  (Body-F) flux-based formulation (Eq. (25));

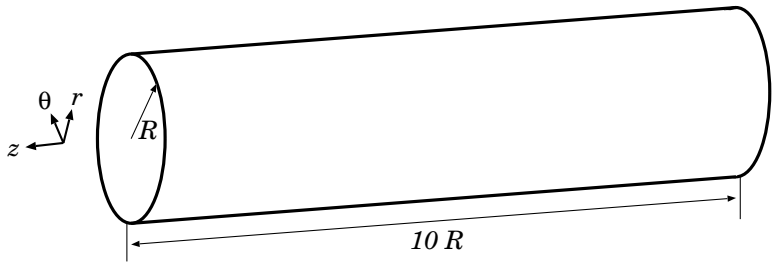

FIG. 5. Computational domain.

- treatment at the cylindrical axis:
  (Axis-C) present procedure (Eqs. (28)–(29)),
  (Axis-E) treatment by Eggels *et al.* [11] (Eq. (23)),
  (Axis-F) method equivalent to flux-based formulation (Eq. (26)).

The computational domain has a radius of $R = 1$ and a length of $10R$ as shown in Fig. 5 and the periodic boundary condition is applied at both ends. Equally spaced and unequally spaced computational meshes are tested. The number and sizes of the computational meshes used in the main test are tabulated in Table 1. The initial velocity field, with which the time-advancing integration is started, is generated in the following way:

1. Interpolate velocities from an instantaneous velocity field of fully developed turbulent pipe flow at $Re_\tau = 180$ simulated on a $96 \times 128 \times 256$ mesh (see the Appendix) onto the mesh (eight times coarser in each direction) used for the tests.

2. Solve the Poisson equation in order for the reduced velocity field to satisfy the continuity equation.

3. Normalize the velocities to have zero mean velocity, i.e., $\langle u_r \rangle = \langle u_\theta \rangle = \langle u_z \rangle = 0$, and unit kinetic energy, i.e., $\langle k \rangle = \langle \frac{1}{2}(u_i u_i) \rangle = 1$.

The procedure employed here is similar to that used by Morinishi *et al.* [8], who used a random stream function in a two-dimensional problem. Instead of using random vector potential as a seed, DNS data are used to obtain an organized three-dimensional velocity field.

Time integration of the discretized equation is achieved by using the low storage third-order Runge–Kutta scheme [19]. The same coefficients as those used by Rai and Moin [20] are used. For the pressure coupling, a delta-form fractional step method, which can be found in [13, 21], is used. The Poisson equation is solved using trigonometric expansions.

Even if the spatial discretization ideally satisfies the energy conservation, the energy may change due to the imperfectness of a time integration scheme. Therefore, a preliminary test is made with different computational time steps of $\Delta t = 0.01$, 0.001, and 0.0001. The

TABLE I
Computational Mesh Used in the Numerical Test

Notation	N_r	N_θ	N_z	Δr	$\Delta\theta$	Δz	χ
Equally spaced	12	16	32	0.083	0.39	0.31	1.00
Unequally spaced	12	16	32	0.021–0.13	0.39	0.31	0.83–1.00

Note. Sizes are nondimensionalized by R. Normalization factor, χ, is defined in Eq. (14).

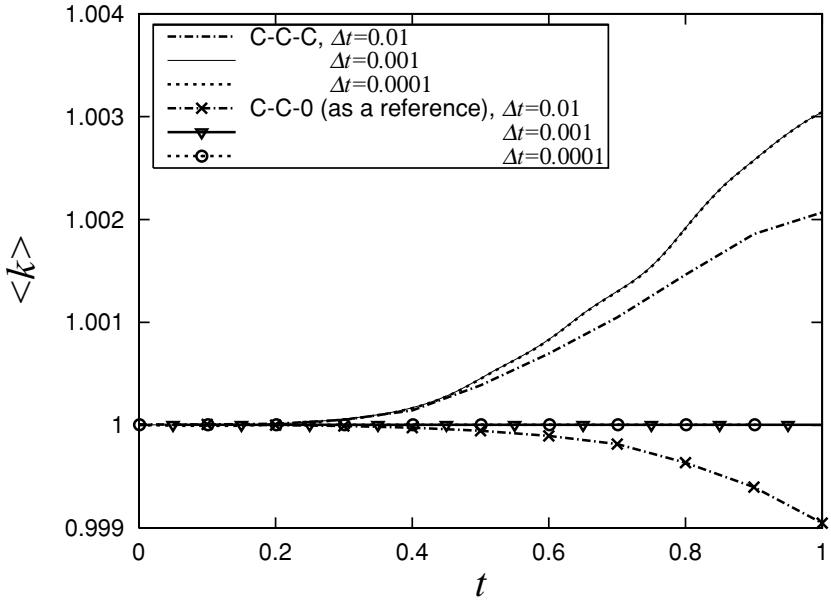

FIG. 6. Time trace of the total kinetic energy $\langle k \rangle$ computed with various time steps. An energy-conservative scheme with (Div.-C)–(Body-C)–(Axis-C) ("C-C-C") and one with a $u_r(0, \theta, z) = 0$ boundary condition ("C-C-0") were used on an equally spaced mesh.

combination of the proposed schemes, i.e., (Div.-C)–(Body-C)–(Axis-C), was used. As discussed in the previous section, (Axis-C) has an imperfect (lower order accuracy) energy-conservation property. Therefore, a case with a boundary condition of $u_r(0, \theta, z) = 0$, denoted as (Axis-0), was also tested in order to examine the case where the problem of the axis treatment is absent. The result is given in Fig. 6, where $\Delta t = 0.001$ and 0.0001 give the indistinguishable results of the kinetic energy, $\langle k \rangle$. Due to the dissipative nature of the Runge–Kutta time integration scheme, $\langle k \rangle$ should decrease with time, and the rate of decrease should be higher for larger Δt. The result for the reference case, i.e., (Div.-C)–(Body-C)–(Axis-0), properly shows such a trend. For (Div.-C)–(Body-C)–(Axis-C), however, the kinetic energy increased due to the imperfect conservation in the treatment of the axis. The smaller increase of $\langle k \rangle$ in the case of $\Delta t = 0.01$ is consistent with the dissipative nature of the time integration scheme. Throughout the following test, the time step is fixed at $\Delta t = 0.001$ except for the test on the different amplitude of initial perturbation and grid resolution where the Courant number is set to be approximately the same as in this condition.

The test is initiated from the case of the equally spaced mesh. Figure 7 shows the time trace of $\langle k \rangle$ in the case of the equally spaced mesh. The kinetic energy should be unchanged as time advances, because the governing equation does not have any source or dissipative terms. According to Fig. 7a, the energy is kept almost constant regardless of differences in the treatment at the cylindrical axis when the present schemes, (Div-.C) and (Body-C), are used. On the other hand, the increase of $\langle k \rangle$ is remarkable in the cases of arithmetic average, (Div.-A) and (Body-A), and of the flux-based formulation, (Div.-F) and (Body-F). Over longer integration times, the increase of $\langle k \rangle$ is discernible in all cases of combination, as shown in Fig. 7b. The present combination, (Div.-C)–(Body-C)–(Axis-C), exhibits the least error in the energy-conservation property and the highest stability. The gradual increase of

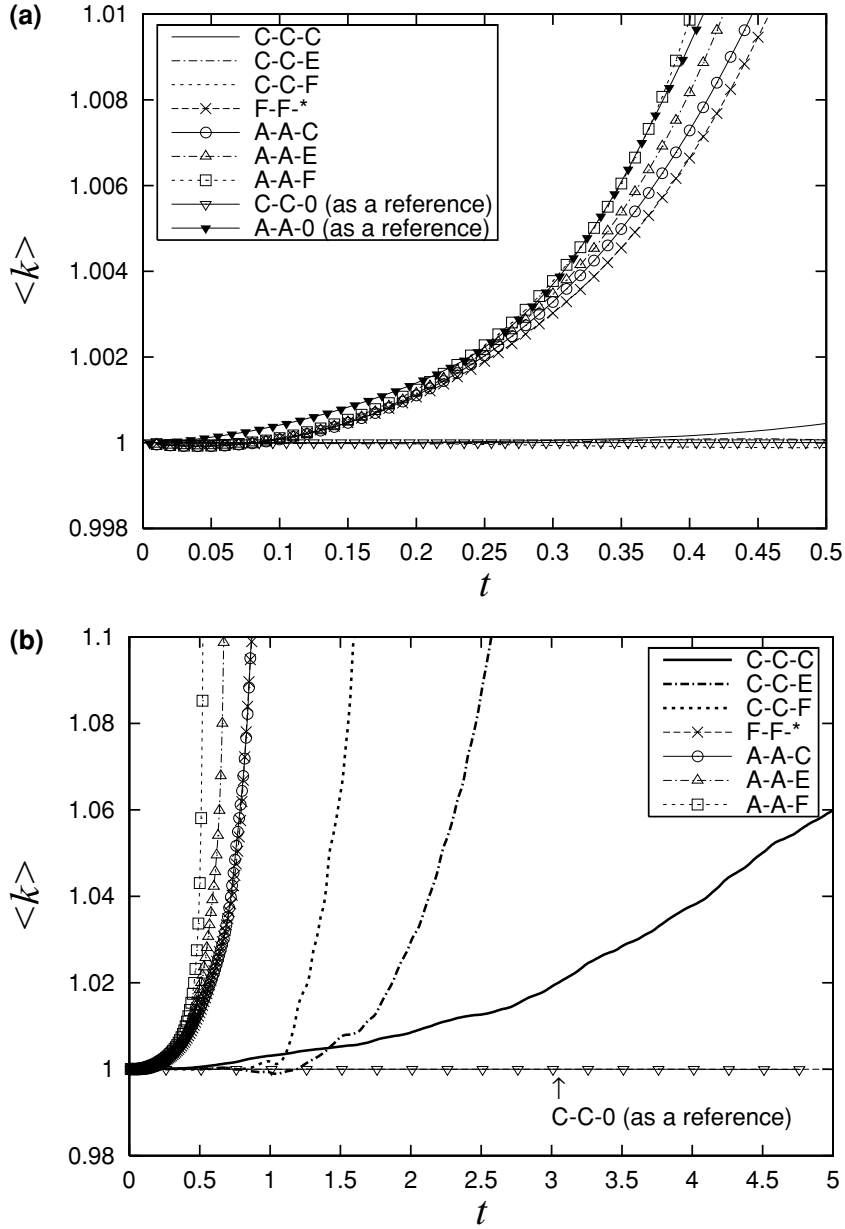

FIG. 7. Time trace of the total kinetic energy $\langle k \rangle$ computed using various methods. (a) Initial period until $t = 0.5$; (b) for longer period until $t = 5$. Equally spaced mesh and $\Delta t = 0.001$ are employed. "C-C-E" denotes a combination of (Div.-C)–(Body-C)–(Axis-E); similar abbreviations apply to other combinations.

$\langle k \rangle$ even for the best scheme, again, can be attributed to the imperfect energy conservation around the cylindrical axis as can be noticed from the result of (Div.-C)–(Body-C)–(Axis-0), also drawn in Fig. 7b as a reference.

As convenient measures of the energy conservation and of the computational stability, we introduce the time when the error in total kinetic energy grows to 1% ($T_{1\%}$) and to 50% ($T_{50\%}$), and when the computation diverges, T_{div}. They are tabulated in Table II. Again,

TABLE II

The Time When the Error in Total Kinetic Energy Grows to 1% ($T_{1\%}$) and 50% ($T_{50\%}$), and the Time When the Computation Diverges (T_{div})

Advection term	Body force term	Treatment at axis	$T_{1\%}$	$T_{50\%}$	T_{div}
(Div.-C)	(Body-C)	(Axis-C)	2.16	16.08	65.62
(Div.-C)	(Body-A)	(Axis-C)	0.81	4.97	15.22
(Div.-C)	(Body-C)	(Axis-E)	1.67	3.50	5.59
(Div.-C)	(Body-C)	(Axis-F)	1.18	1.93	2.34
(Div.-F)	(Body-F)	$*$	0.46	1.25	1.36
(Div.-A)	(Body-A)	(Axis-C)	0.45	1.02	1.12
(Div.-A)	(Body-C)	(Axis-C)	0.44	0.82	0.86
(Div.-A)	(Body-A)	(Axis-E)	0.43	0.71	0.75
(Div.-A)	(Body-A)	(Axis-F)	0.41	0.55	0.56

Note. Equally spaced mesh and $\Delta t = 0.001$ are employed.

the combination of the present schemes, (Div.-C)–(Body-C)–(Axis-C), is far superior to other combinations. The energy-conservation property is more sensitive to the scheme used for the advection and body force terms than to the treatment at the axis. Moreover, it is noticeable from the comparison between (Div.-C)–(Body-A)–(Axis-C) and (Div.-A)–(Body-C)–(Axis-C) that the energy conservation of the advection term is more important than that of the body force term.

Dependency of the energy-conservation property in an initial period, $t = 0.25$ (corresponding to the center of Fig. 7a), on the amplitude of initial perturbation, $\langle k \rangle_{init}$, and the grid resolution, Δr, is depicted in Fig. 8. The error, ε, is defined as

$$\varepsilon = \frac{\langle k \rangle_{t=0.25} - \langle k \rangle_{init}}{\langle k \rangle_{init}}. \tag{39}$$

It is reconfirmed that the error of the proposed scheme, i.e., (Div.-C)–(Body-C)–(Axis-C),

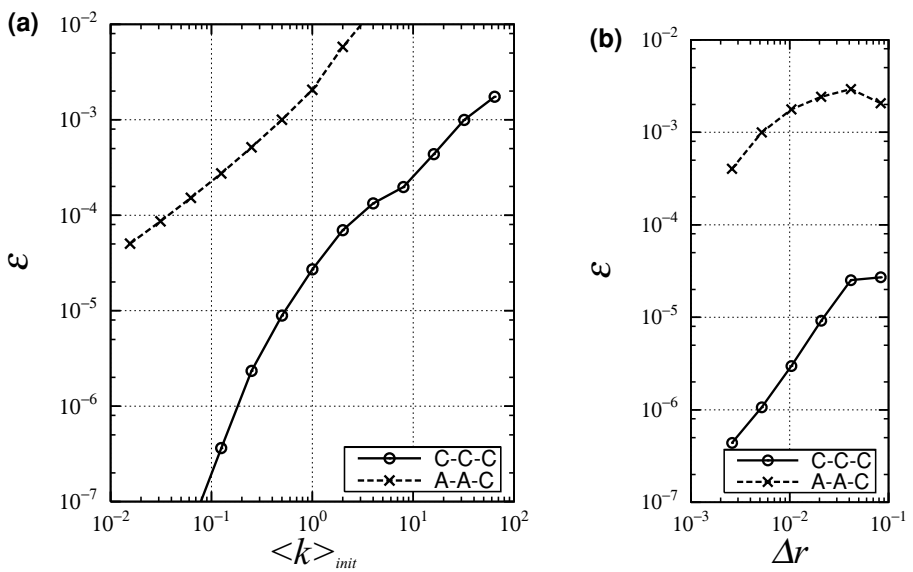

FIG. 8. Dependency of the error in kinetic energy in an initial period ($t = 0.25$), (a) on the amplitude of initial perturbation and (b) on the grid size.

TABLE III
The Time When the Error in Total Kinetic Energy Grows to 1% ($T_{1\%}$) and 50% ($T_{50\%}$), and When the Computation Diverges, T_{div}

Advection term	Body force term	Treatment at axis	$T_{1\%}$	$T_{50\%}$	T_{div}
(Div.-C)	(Body-C)	(Axis-C)	2.71	34.16	167.13
(Div.-F)	(Body-F)	*	0.50	1.47	1.52
(Div.-A)	(Body-A)	(Axis-C)	0.49	1.44	1.56

Note. Unequally spaced mesh and $\Delta t = 0.001$ are employed.

is much smaller than that of the intuitive scheme, i.e., (Div.-A)–(Body-A)–(Axis-C), for any $\langle k \rangle_{init}$ and Δr. The error decreases as $\langle k \rangle_{init}$ or Δr becomes smaller. The energy- conservation property of the present scheme is found to be between first and second order in terms of Δr which reflects the order of inconsistency in (Axis-C). It should be noted that the error in the reference case, (Div.-C)–(Body-C)–(Axis-0), is much smaller, and most of that error is likely caused by the time integration ($\varepsilon \simeq -3 \times 10^{-8}$ for $\langle k \rangle_{init} = 1$ and $\Delta r \simeq 0.083$).

Subsequently, a test on the unequally spaced mesh is performed with the default conditions, i.e., $\langle k \rangle_{init} = 1$ and the mesh shown in Table I. As summarized in Table III, the results are similar to those for the equally spaced mesh. The energy-conservation property of the present scheme for the advection term is quite good despite the approximation of $\chi = 1$ made in the verification process (Eqs. (15)–(17)), and the superiority of the combination of the present schemes is even clearer. Given the comparison between Tables II and III, one may wonder why the error computed using the present schemes grows more slowly on the unequally spaced mesh. Note that these two results cannot be directly compared because the smoothness of the initial fields is different. Comparison between tests with different mesh sizes is not straightforward in the case of unequally spaced mesh and is thus omitted. However, it is apparent from Eqs. (7) and (11) that the difference between the intuitive scheme and the present scheme becomes smaller as $\Delta r \to 0$.

6. CONCLUSIONS

Investigations were made on the energy conservation of second-order-accurate finite difference schemes for a cylindrical coordinate system. A combination of highly energy-conservative schemes for advection and centrifugal/Coriolis terms and the treatment of the singularity at the cylindrical axis was proposed.

Similar to the case of the Cartesian coordinate system, the energy-conservative scheme for advection terms can be formulated by using relevant interpolation schemes. However, unlike in the Cartesian coordinate system [9], the resulting form of the energy-conservative scheme differs from that of an intuitive scheme based on arithmetic average, even when the mesh is equally spaced.

The proposed schemes are tested numerically via simulations of inviscid flow. The highly energy-conservative nature and the high stability of the present schemes over other schemes are demonstrated.

The strict energy conservation discussed in the present paper may not be required for DNS of a fully developed turbulent flow, as indicated in the Appendix, where a very

fine mesh is used and large physical dissipation takes place. However, the energy conservation will become important in many other situations such as LES using coarse mesh and DNS of statistically unstationary turbulent flow due, for example, to external control input.

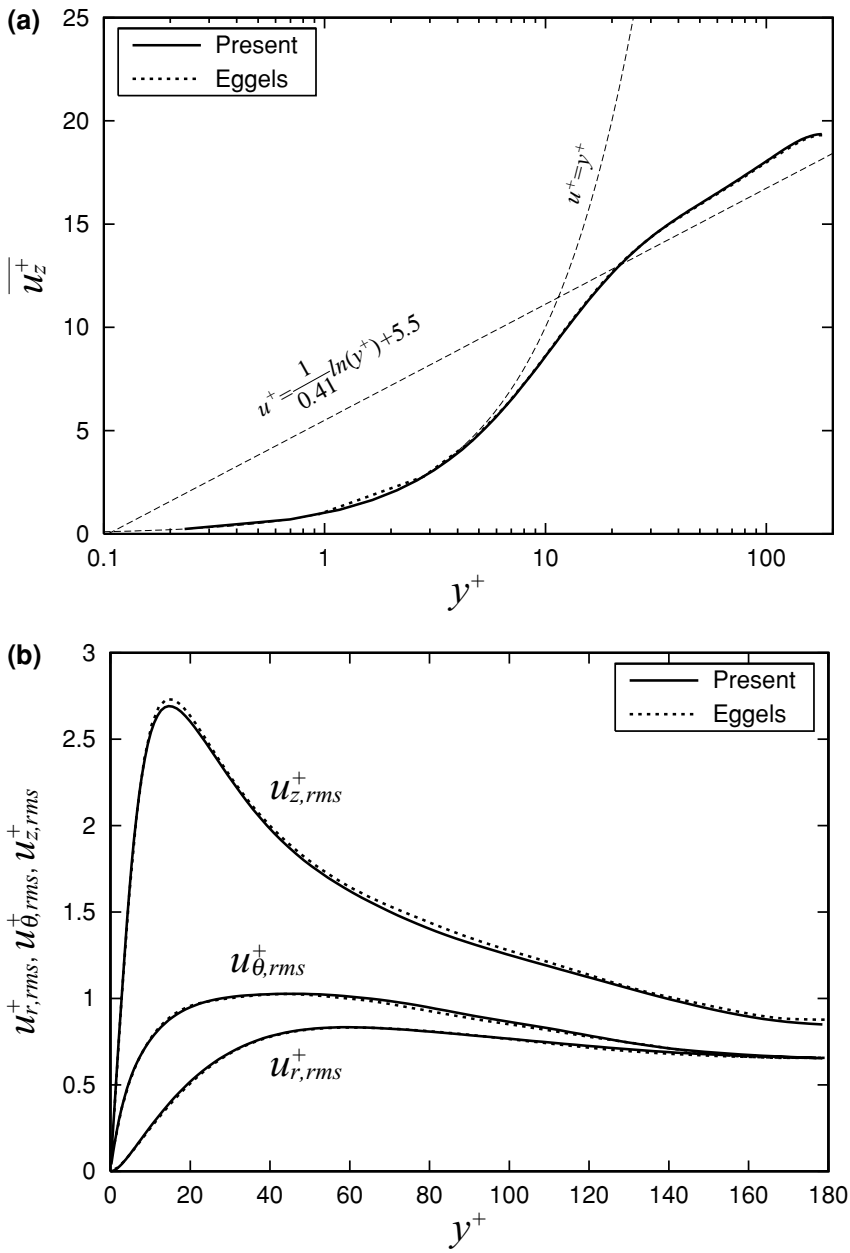

FIG. 9. Typical results from DNS of turbulent pipe flow at $Re_\tau = 180$. (a) Mean velocity profile; (b) RMS velocity fluctuations; (c) limiting behavior of Reynolds stresses; (d) turbulent kinetic energy budget. Present results are compared with DNS data by Eggels *et al.* [11], Unger and Friedrich (in [11]), and DNS data of channel flow by Moser *et al.* [22].

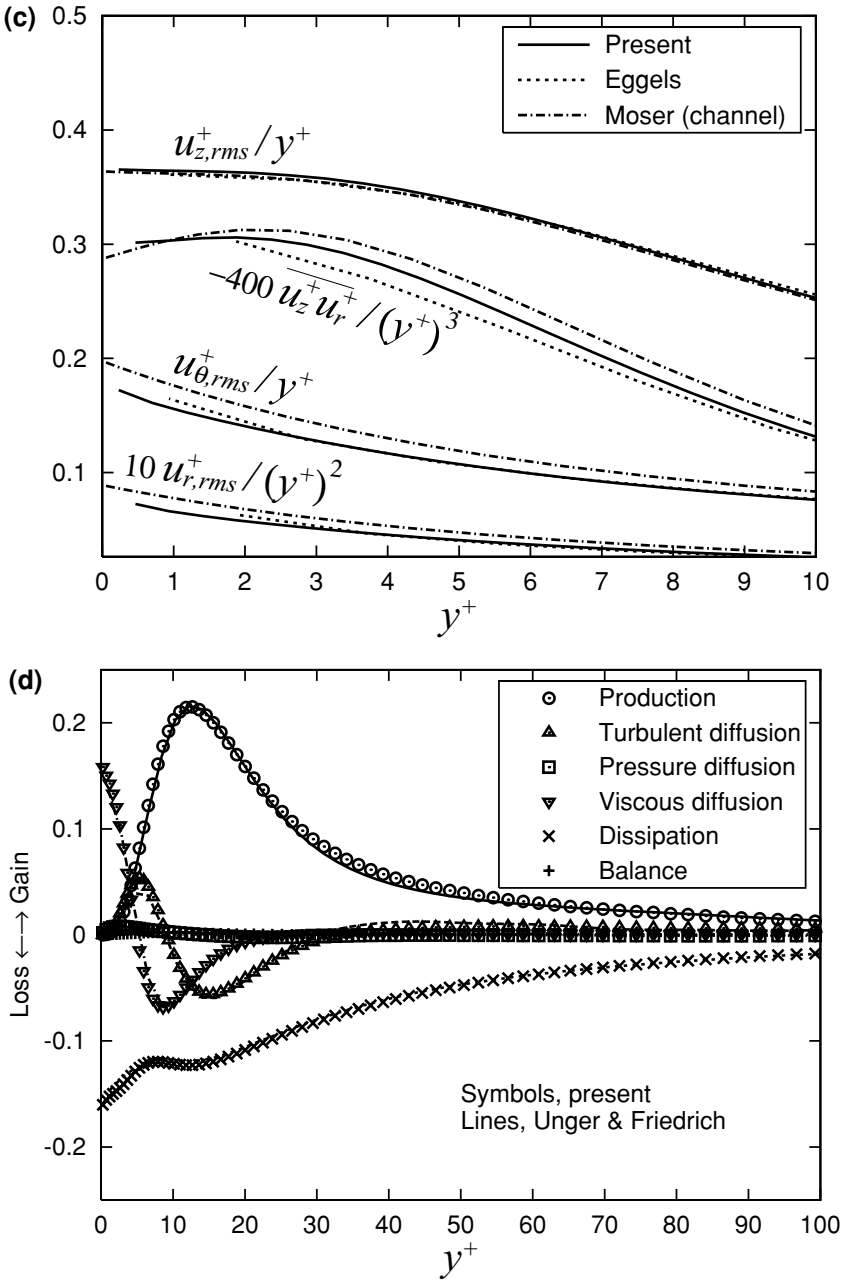

FIG. 9—*Continued*

APPENDIX: DNS OF FULLY DEVELOPED TURBULENT PIPE FLOW

As an initial field in test computations, an instantaneous velocity field of a fully developed turbulent pipe flow was used. In this Appendix, some results from DNS of turbulent pipe flow at $Re_\tau = u_\tau R/\nu = 180$ are presented to show the accuracy of the present computation.

For the discretization of governing equations (1) and (2), the methods proposed in the present study, i.e., (Div.-C), (Body-C), and (Axis-C), are used. The diffusion terms are

spatially discretized using an ordinary second-order accurate finite difference and integrated in time using a Crank–Nicolson scheme. The length of the computational domain is $10R$. The computational mesh is $96 \times 128 \times 256$ and stretched in the r direction from $\Delta r^+ = 0.46$ (wall) to $\Delta r^+ = 2.99$ (center). The computational time step is $\Delta t^+ = 0.18$.

As representative quantities, profiles of the mean velocity and the RMS velocity fluctuations, the limiting behavior of Reynolds stresses, and the budget of kinetic energy are shown in Fig. 9. The present results agree well with available DNS data. All the other quantities which are not shown here are also in good agreement, with slight differences in the vicinity of the wall, as in Fig. 9c, due to the difference of resolution.

Turbulence statistics, Reynolds stress budgets, two-point correlations, and one-dimensional energy spectra computed by the present DNS are available in tabulated forms at the website (`http://www.thtlab.t.u-tokyo.ac.jp/`).

ACKNOWLEDGMENT

This work was supported through the Project for Organized Research Combination System by the Ministry of Education, Culture, Sports, and Technology of Japan (MEXT).

REFERENCES

1. M. Lesieur and O. Métais, New trends in large-eddy simulations of turbulence, *Annu. Rev. Fluid Mech.* **28**, 45 (1996).
2. U. Piomelli, Large-eddy simulations: Where we stand, in *Advances in DNS/LES* edited by C. Liu, Z. Liu, and L. Sakell (Greyden Press, Columbus, 1997), p. 93.
3. N. Kasagi, Progress in direct numerical simulation of turbulent transport and its control, *Int. J. Heat Fluid Flow* **19**, 125 (1998).
4. P. Moin and K. Mahesh, Direct numerical simulation: A tool in turbulence research, *Annu. Rev. Fluid Mech.* **30**, 539 (1998).
5. D. Gottlieb and S. A. Orszag, *Numerical Analysis of Spectral Methods: Theory and Applications* (Soc. for Industr. & Appl. Math. Philadelphia, 1977).
6. F. H. Harlow and J. E. Welch, Numerical calculation of time-dependent viscous incompressible flow of fluid with free surface, *Phys. Fluids* **8**, 2182 (1965).
7. S. A. Piacsek and G. P. Williams, Conservation properties of convection difference schemes, *J. Comput. Phys.* **6**, 392 (1970).
8. Y. Morinishi, T. S. Lund, O. V. Vasilyev, and P. Moin, Fully conservative higher order finite difference schemes for incompressible flow, *J. Comput. Phys.* **143**, 90 (1998), doi:10.1006/jcph.1998.5962.
9. T. Kajishima, Finite-difference method for convective terms using non-uniform grid, *Trans. JSME/B* **65**(633), 103 (1999) (in Japanese).
10. F. E. Ham, F. S. Lien, and A. B. Strong, A fully conservative second-order finite difference scheme for incompressible flow on nonuniform grids, *J. Comput. Phys.* **177**, 117 (2002), doi:10.1006/jcph.2002.7006.
11. J. G. M. Eggels, F. Unger, M. H. Weiss, J. Westerweel, R. J. Adrian, R. Friedrich, and F. T. M. Nieuwstadt, Fully developed turbulent pipe flow: A comparison between direct numerical simulation and experiment, *J. Fluid Mech.* **268**, 175 (1994).
12. K. Akselvoll and P. Moin, *Large Eddy Simulation of Turbulent Confined Coannular Jets and Turbulent Flow over a Backward Facing Step*, Stanford Univ. Report TF-63 (1995).
13. R. Verzicco and P. Orlandi, A finite-difference scheme for three-dimensional incompressible flows in cylindrical coordinates, *J. Comput Phys.* **123**, 402 (1996), doi:10.1006/jcph.1996.0033.
14. P. Orlandi and M. Fatica, Direct simulations of turbulent flow in a pipe rotating about its axis, *J. Fluid Mech.* **343**, 43 (1997).

15. G. S. Constantinescu and S. K. Lele, A new method for accurate treatment of flow equations in cylindrical coordinates using series expansions, in *CTR Annual Research Briefs 2000*, edited by P. Moin, W. C. Reynolds, and N. N. Mansour (Center for Turbulence Research, NASA Ames and Stanford Univ. Press, Stanford, CA, 2000), p.199.
16. K. Mohseni and T. Colonius, Numerical treatment of polar coordinate singularities, *J. Comput. Phys.* **157**, 787 (2000), doi:10.1006/jcph.1999.6382.
17. O. Vasilyev, High order finite difference schemes on non-uniform meshes with good conservation properties, *J. Comput. Phys.* **157**, 746 (2000), doi:10.1006/jcph.1999.6398.
18. J. P. Boyd, *Chebyshev and Fourier Spectral Methods* (Springer-Verlag, Berlin, 1989), p. 475.
19. P. R. Spalart, R. D. Moser, and M. M. Rogers, Spectral methods for the Navier–Stokes equations with one infinite and two periodic directions, *J. Comput. Phys.* **96**, 297 (1991).
20. M. M. Rai and P. Moin, Direct numerical simulations of turbulent flow using finite difference schemes, *J. Comput. Phys.* **96**, 15 (1991).
21. J. K. Dukowicz and A. S. Dvinsky, Approximate factorization as a higher order splitting for the implicit incompressible flow equations, *J. Comput. Phys.* **102**, 336 (1992).
22. R. D. Moser, J. Kim, and N. N. Mansour, Direct numerical simulation of turbulent channel flow up to $Re_\tau = 590$, *Phys. Fluids* **11**, 943 (1999).